River Flow 2010 - Dittrich, Koll, Aberle & Geisenhainer (eds) - © 2010 Bundesanstalt für Wasserbau ISBN 978-3-939230-00-7

Laboratory experiments on gravity currents moving on smooth and rough beds

C. Adduce, V. Lombardi, G. Sciortino & M. La Rocca
Department of Civil Engineering, University Roma Tre, Rome, Italy

ABSTRACT: The aim of this paper is the investigation of gravity currents moving on both smooth and rough beds by laboratory experiments. Gravity currents were produced in a Perspex tank of rectangular cross-section by lock exchange release experiments. The tank is divided into two parts by a sliding gate: one filled with tap water and the other one filled with salt water to the same height. Nine experiments were performed varying both the bed roughness and the initial density of the gravity current. All the experiments were recorded by a camera and an image analysis technique was applied to measure the space-time evolution of the gravity current's profile. For the experiments with a smooth bed three different phases were observed in the gravity current's dynamics: a first slumping or constant speed phase; a second self-similar phase, in which the front speed decreased as $t^{-1/3}$, where t is the time measured from release; a third viscous phase, in which the front velocity decreased as $t^{-4/5}$. In the experiments performed with a rough bed the measured front's velocities were observed to be lower than the front's velocity of gravity currents moving on a smooth bed.

Keywords: Gravity currents, Bed roughness, Laboratory tests

1 INTRODUCTION

Gravity currents occur when a fluid flows into another fluid with a different density. The density gradient can be due to a difference of temperature, salinity or to the presence of suspended sediments (i.e. turbidity currents). These phenomena are very common in natural flows as avalanches, pyroclastic flows, sea breeze winds, oceans' gravity currents. A large variety of examples of gravity currents can be found in Simpson (1997).

Several authors studied the dynamics of gravity currents with both numerical and experimental analysis. Most of the models simulating gravity currents are based on the shallow water approximation as Rottman & Simpson (1983), Shin et al. (2004), La Rocca et al. (2008) and Adduce et al. (2009). When a gravity current moves inside an ambient fluid, it mixes with the surrounding fluid. A recent investigation on the parametrization of mixing due to gravity currents is given by Cenedese and Adduce (2008).

An experimental technique used to produce a gravity current is the lock-exchange release. In this configuration the tank is divided in two portion separated by a vertical sliding gate, one filled with tap water, and the other filled with salt water, as shown in Figure 1. The experiment begins when the gate is suddenly removed and the heavier fluid (salty water) flows under the lighter one (fresh water), producing a gravity current. The experiment stops when the current's front reaches the right end wall of the tank.

The dynamics of gravity currents, obtained by an instantaneous release, can be divided into three different phases (Simpson 1997; Marino et al., 2005). During the first phase, called slumping phase, the front position varies linearly with time and the front speed is constant. Rottman & Simpson (1983) found that the first phase stops at a distance from the left wall, l_s, given by

$$x_f = l_s \cong 10 \cdot x_0 \tag{1}$$

where x_f is the front position, x_0 is a length scale defined as the distance between the gate and the left vertical wall of the tank.

During the second phase or self-similar phase the front speed U_f varies with $t^{-1/3}$ (i.e. the front position depends on time by a law $t^{2/3}$). The transition to the second phase occurs when a wave,

caused by the reflection of the lighter fluid to the left wall, reaches the current's front, which is slower than the wave.

The third phase or viscous phase occurs if viscous effects become predominant. Huppert (1982) found that the transition between the self-similar phase and the viscous phase is reached when $x_f \cong l^*$ with l^* defined as

$$l^* = \left(\frac{g_0' h_0^5 x_0^5}{\nu^2} \right)^{\frac{1}{7}} \quad (2)$$

where h_0 is the initial depth of the lighter fluid, ν is the kinematic viscosity of the heavier fluid and g_0' is the initial reduced gravity, defined as

$$g_0' = g \frac{\rho_{01} - \rho_2}{\rho_2} \quad (3)$$

where ρ_{01} is the initial density of the gravity current, ρ_2 is the density of the heavier fluid and g is the gravity acceleration.

The aim of this paper is the investigation of gravity currents moving on beds with different roughness by laboratory experiments.

Nine laboratory experiments were performed by a lock release with three bed's roughness $\varepsilon \cong 0$ mm, 2.2 mm e 4.5 mm and three values of initial density $\rho_{01} \cong 1009$ Kg/m^3, 1024 Kg/m^3 and 1060 Kg/m^3.

The observed general trend is that an increase of bed's roughness causes a decrease of the front speed.

2 EXPERIMENTAL SET-UP

The experiments were performed at the Hydraulics Laboratory of University Roma Tre, in a Perspex tank of rectangular cross-section, 300 cm long, 30 cm deep and 20 cm wide. A sketch of the tank is shown in Figure 1.

The tank was divided into two parts by a sliding vertical gate placed at a distance x_0 from the left end wall of the tank. The right portion was filled with tap water of density ρ_2, while the left part was filled with salty water with initial density $\rho_{01} > \rho_2$. Both in the right and in the left part of the tank the depth of the fluid was h_0.

A pycnometer was used to perform density measurements. A quantity of dye was dissolved into the salt water to allow the visualization of the gravity current.

The experiment begins when the sliding gate is suddenly removed and the heavier fluid moves from the left part of the tank to the right part forming a gravity current. The time needed to remove the gate is about 0.5 s. The experiment stops when the front of the gravity current reaches the right wall of the tank.

The desired bed's roughness ε was obtained gluing sand of a defined mean diameter on the bottom of the tank.

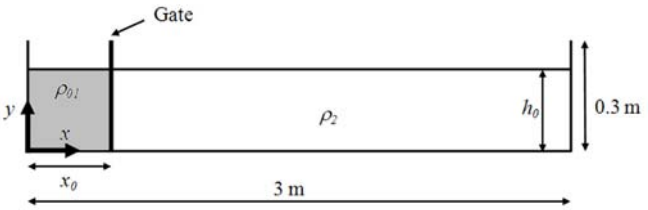

Figure 1. Definition sketch of the tank used for the experiments.

A CCD camera, with a frequency of 25 Hz, was used to record the experiments and an image analysis technique, based on a threshold method, was applied to measure the space-time evolution of the gravity currents.

Each acquired image is a matrix of pixels, each of which is characterized by a number ranging from 0 (black) to 255 (white). The grey level typical of the interface between the two fluids was chosen as a threshold value. The program travelled along the columns of the matrix until it met the threshold value (i.e. the interface between the two fluids) and recorded the coordinates of this pixel as a point of the current's profile.

A rule was positioned along both the horizontal and vertical walls of the tank in order to obtain the conversion factor pixel/cm.

Figure 2 shows for run 7 the measured current's profiles overlapping the images captured for the camera for three different time steps.

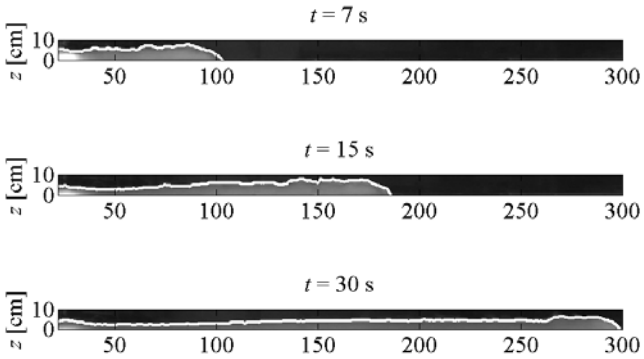

Figure 2. Gravity current's profile (white line) overlapping the images captured by the camera for RUN 7 at 7 s, 15 s and 30 s after release.

Nine experiments were performed keeping constant $\rho_2 = 1000$ Kg/m^3, $h_0 = 0.15$ m, $x_0 = 0.10$ m and varying the bed's roughness ε and gravity current's initial density ρ_{01}. The experimental parameters are shown in Table1.

Table 1. Experimental parameters

RUN	ρ_{01}[Kg/m^3]	ε [mm]
1	1009.3	0
2	1009.2	2.2
3	1008.8	4.5
4	1023.7	0
5	1024.4	2.2
6	1023.7	4.5
7	1059.6	0
8	1060.0	2.2
9	1059.5	4.5

3 LABORATORY EXPERIMENTS

In Figure 3a-c experimental front's positions versus time are shown for all the performed runs. The maximum front's position was always at the flume bed. The observed trend is that the speed of the gravity currents decreases as the bed roughness increases.

Figure 4a-c shows the measured gravity current's profiles obtained with the threshold's method for all the performed runs at three different time steps after release.

All laboratory measurements start about 2 seconds after the gate removal, because of the very chaotic behavior during the first stage of gravity current's dynamics.

Figure 4a shows the experimental profiles for the runs performed with $\rho_{01} \cong 1009$ Kg/m^3: 12 s after the gate removal, the gravity currents for the runs 1, 2, and 3 covered a distance of 85 cm, 82 cm and 72 cm respectively; after 20 s the currents covered a distance of 127 cm, 125 cm, 109 cm; at least after 37 s the currents covered a distance of 198 cm, 191 cm and 174 cm.

Figure 4b shows the experimental profiles for the runs performed with $\rho_{01} \cong 1024$ Kg/m^3: 12 s after the gate removal, the gravity currents for the runs 4, 5, and 6 covered a distance of 113 cm, 102 cm and 101 cm respectively; after 20 s the currents covered a distance of 169 cm, 155 cm, 149 cm; at least after 37 s the currents covered a distance of 262 cm, 240 cm and 224 cm.

Figure 4c shows the experimental profiles for the runs performed with $\rho_{01} \cong 1060$ Kg/m^3: 12 s after the gate removal, the gravity currents corresponding to the runs 7, 8, and 9 covered a distance of 155 cm, 147 cm and 141 cm respectively; after 20 s the currents covered a distance of 228 cm, 209 cm, 206 cm; at least after 37 s the currents covered a distance of 298 cm, 265 cm and 262 cm. As the bed roughness increases, the velocity of the gravity currents decreases.

For a constant time, the gravity currents moving on a smooth bed cover a longer distance than those moving on rough beds.

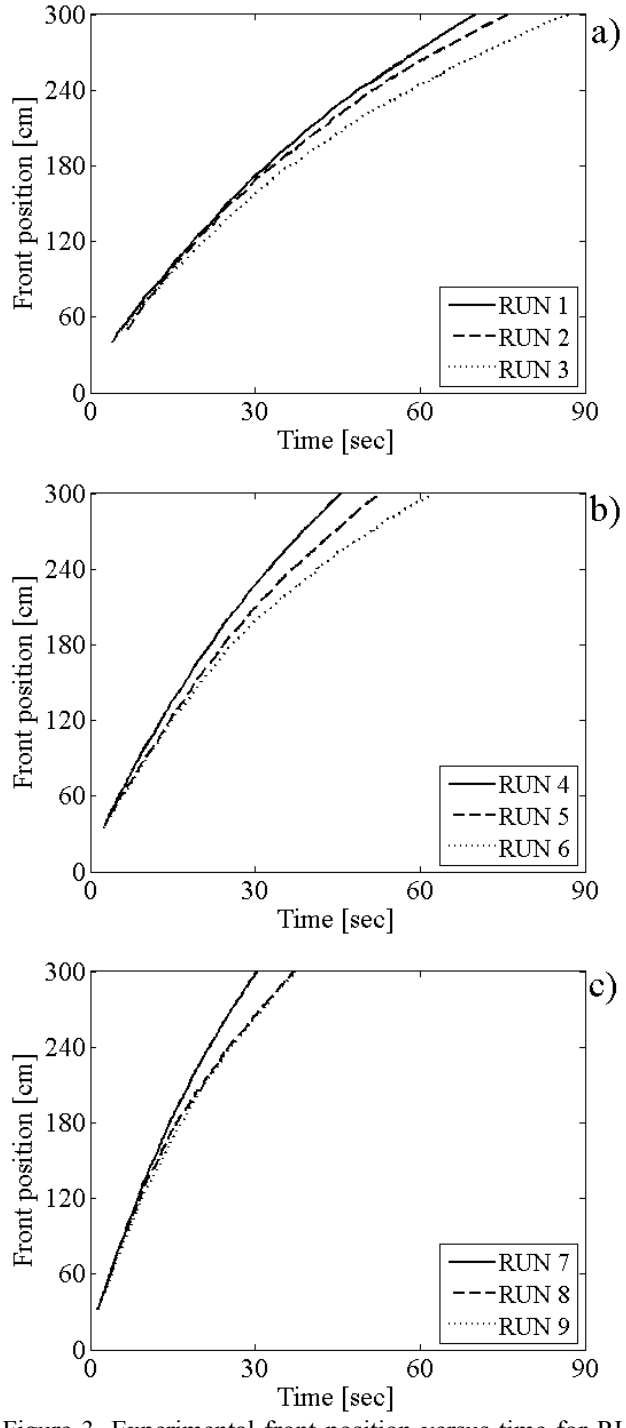

Figure 3. Experimental front position versus time for RUN 1, 2, 3 ($\rho_{01} \cong 1009$ Kg/m^3) (a), RUN 4, 5, 6 ($\rho_{01} \cong 1024$ Kg/m^3) (b), RUN 7, 8, 9 ($\rho_{01} \cong 1060$ Kg/m^3) (c).

The three phases developing in a gravity current are described in section 1. The lengths of the slumping, self-similar and viscous phase were computed for the gravity currents performed with $\varepsilon = 0$ mm and $\varepsilon = 4.5$ mm, following the relations found in the literature.

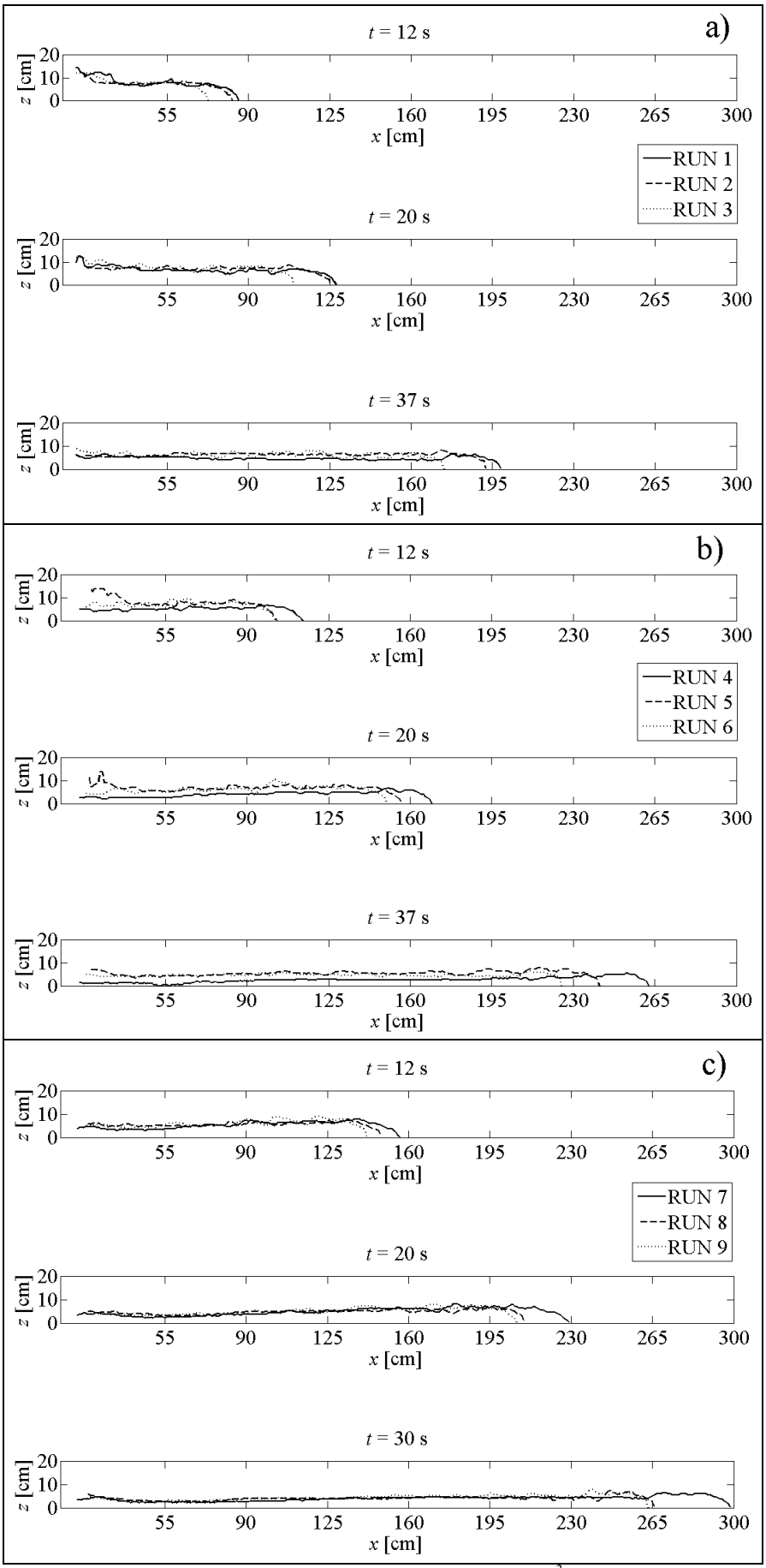

Figure 4. Measured gravity current's profiles for RUN 1, 2, 3 ($\rho_{01} \cong 1009$ Kg/m^3) (a), RUN 4, 5, 6 ($\rho_{01} \cong 1024$ Kg/m^3) (b), RUN 7, 8, 9 ($\rho_{01} \cong 1060$ Kg/m^3) (c) at different time steps.

The dimensionless front position versus dimensionless time for gravity currents moving on a smooth bed and those obtained with $\varepsilon = 4.5$ mm and the three regression lines, obtained by the

formulae found in the literature, for the linear, self-similar and viscous phase are respectively shown in Figure 5a-c and 6a-c. The length scale x_0 is the gate position, while the time scale t_0 is defined as

$$t_0 = \frac{x_0}{\sqrt{h_0 g_0'}} \tag{4}$$

The length of the slumping phase l_s can be calculated following Rottman & Simpson (1983) by Equation (1). The distance at which a transition between the linear and self-similar phase occurs is indicated by circles in Figures 5a-c and 6a-c. The distance at which the viscous phase starts l^*, shown by triangles in Figures 5a-c and 6a-c, is calculated following Huppert (1982) by Equation (2). The length of the viscous phase l_{vis} is given by the difference between the total length of the tank and the distance at which the third phase starts. The length of the self-similar phase l_{ss} can be obtained by the difference between l^* and l_s. In table 2 l_s, l_{ss}, l_{vis} for the runs performed with ε = 0 mm and ε = 4.5 mm are shown.

In agreement with the literature, the linear phase, the self-similar phase and the viscous phase can be regressed by a linear law, by a power law with $(t/t_0)^{2/3}$ and by a power law with $(t/t_0)^{2/3}$, respectively. The obtained three regression curves for each phase of Run 1, Run 4 and Run 7 (i.e. ε = 0 mm) and for Run 3, Run 6, and Run 9 (i.e. ε = 4.5 mm) are given by the sets of equations (5)-(10). The coefficients of determination R^2 has been also calculated for the three phases. The dimensionless plots are in agreement with previous formulae by Rottman & Simpson (1983) and by Huppert (1982).

$$\begin{cases} \dfrac{x_f - x_0}{x_0} = 1.065 + 0.461\dfrac{t}{t_0} & R^2 = 0.998 \\ \dfrac{x_f - x_0}{x_0} = -2.962 + 1.782\left(\dfrac{t}{t_0}\right)^{\frac{2}{3}} & R^2 = 0.999 \\ \dfrac{x_f - x_0}{x_0} = -54.74 + 34.631\left(\dfrac{t}{t_0}\right)^{\frac{1}{5}} & R^2 = 0.999 \end{cases} \tag{5}$$

$$\begin{cases} \dfrac{x_f - x_0}{x_0} = 0.721 + 0.437\dfrac{t}{t_0} & R^2 = 0.998 \\ \dfrac{x_f - x_0}{x_0} = -3.301 + 1.714\left(\dfrac{t}{t_0}\right)^{\frac{2}{3}} & R^2 = 0.999 \\ \dfrac{x_f - x_0}{x_0} = -60.886 + 36.906\left(\dfrac{t}{t_0}\right)^{\frac{1}{5}} & R^2 = 0.999 \end{cases} \tag{6}$$

$$\begin{cases} \dfrac{x_f - x_0}{x_0} = 0.606 + 0.413\dfrac{t}{t_0} & R^2 = 0.998 \\ \dfrac{x_f - x_0}{x_0} = -3.105 + 1.635\left(\dfrac{t}{t_0}\right)^{\frac{2}{3}} & R^2 = 0.999 \\ \dfrac{x_f - x_0}{x_0} = -62.582 + 37.226\left(\dfrac{t}{t_0}\right)^{\frac{1}{5}} & R^2 = 0.999 \end{cases} \tag{7}$$

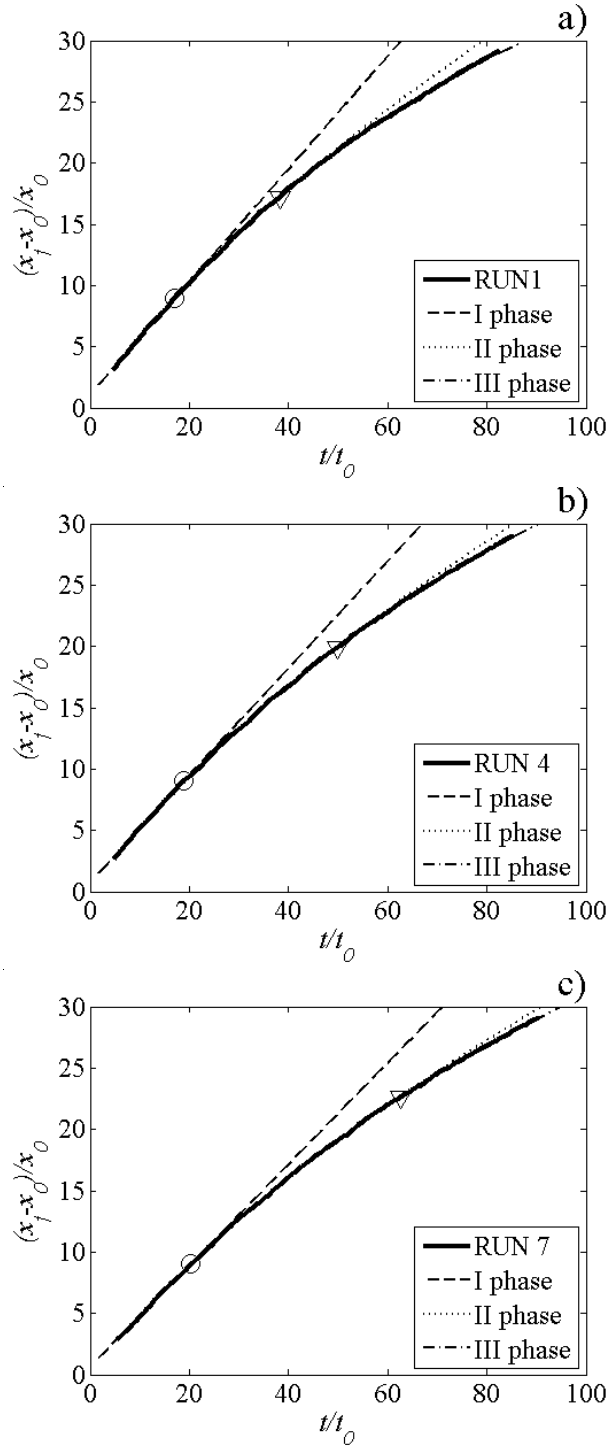

Figure 5. Dimensionless front position versus dimensionless time for RUN 1 (a), RUN 4 (b), RUN 7 (c) and regression lines for I phase (linear phase), II phase (self-similar phase) and III phase (viscous phase).

Table 2. Lengths of the three phases of gravity current's dynamics evaluated by the formulae for a smooth bed.

Run	l_s [m]	l_{ss} [m]	l_{vis} [m]
1	1	0.831	1.169
3	1	0.816	1.184
4	1	1.094	0.906
6	1	1.094	0.906
7	1	1.389	0.611
9	1	1.388	0.612

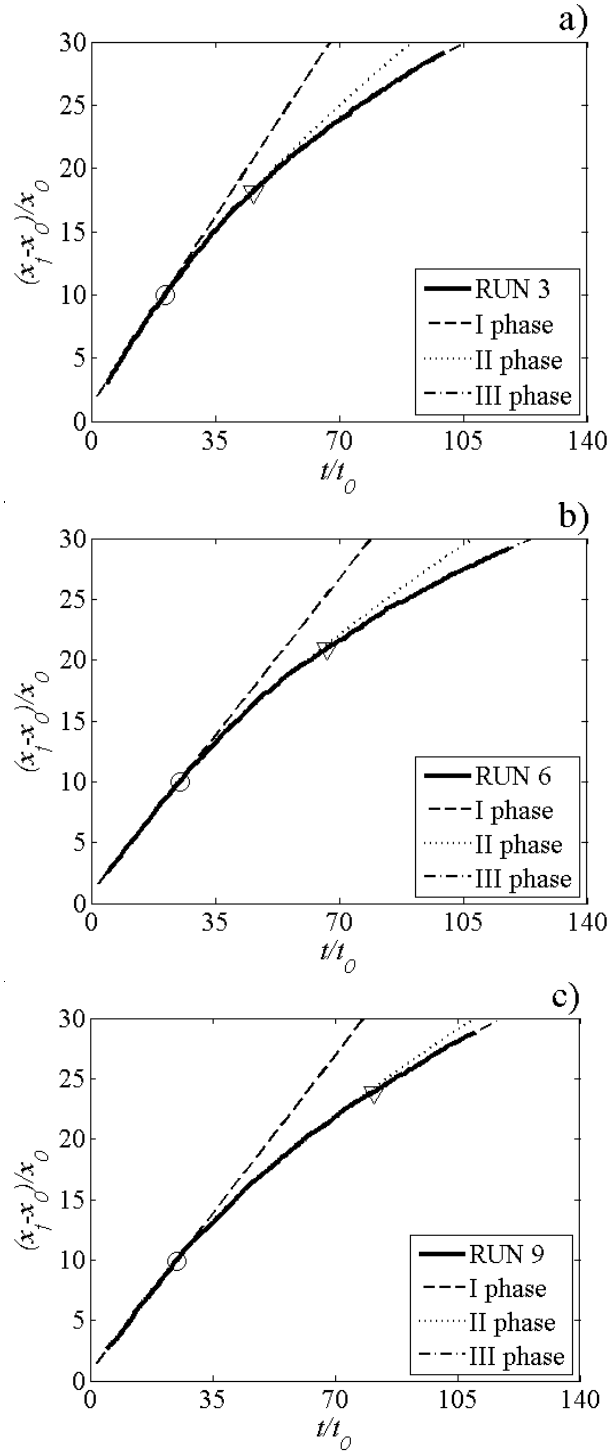

Figure 6. Dimensionless front position versus dimensionless time for RUN 3 (a), RUN 6 (b), RUN 9 (c) and regression lines for I phase (linear phase), II phase (self-similar phase) and III phase (viscous phase).

$$\begin{cases} \dfrac{x_f - x_0}{x_0} = 1.248 + 0.426\dfrac{t}{t_0} & R^2 = 0.997 \\ \dfrac{x_f - x_0}{x_0} = -1.928 + 1.581\left(\dfrac{t}{t_0}\right)^{\frac{2}{3}} & R^2 = 0.999 \\ \dfrac{x_f - x_0}{x_0} = -47.308 + 30.4184\left(\dfrac{t}{t_0}\right)^{\frac{1}{5}} & R^2 = 0.999 \end{cases} \quad (8)$$

$$\begin{cases} \dfrac{x_f - x_0}{x_0} = 0.854 + 0.369\dfrac{t}{t_0} & R^2 = 0.999 \\ \dfrac{x_f - x_0}{x_0} = -1.819 + 1.405\left(\dfrac{t}{t_0}\right)^{\frac{2}{3}} & R^2 = 0.999 \\ \dfrac{x_f - x_0}{x_0} = -47.274 + 29.437\left(\dfrac{t}{t_0}\right)^{\frac{1}{5}} & R^2 = 0.999 \end{cases} \quad (9)$$

$$\begin{cases} \dfrac{x_f - x_0}{x_0} = 0.7.14 + 0.374\dfrac{t}{t_0} & R^2 = 0.999 \\ \dfrac{x_f - x_0}{x_0} = -1.52 + 1.374\left(\dfrac{t}{t_0}\right)^{\frac{2}{3}} & R^2 = 0.999 \\ \dfrac{x_f - x_0}{x_0} = -55.299 + 32.852\left(\dfrac{t}{t_0}\right)^{\frac{1}{5}} & R^2 = 0.999 \end{cases} \quad (10)$$

4 CONCLUSIONS

This paper investigates the effect of bed's roughness on gravity currents' dynamics produced by lock release experiments. Nine laboratory experiments were conducted keeping constant the density of the ambient fluid, the initial height of the two fluids, the initial position of the vertical gate and varying the bed's roughness ε and the gravity current's initial density. Three different values of bed's roughness and three different values of initial density were tested. The space-time evolution of the gravity current's profile was measured by an image analysis technique.

For the currents realized on a smooth bed and for those performed with ε = 4.5 mm, three different phases were observed: a first or constant speed phase, called slumping phase, a second self-similar phase and a third viscous phase. During the second and the third phases the front velocity is observed to decrease as the time increases. Each phase was regressed by different laws in agreement with the literature. For all the experiments performed on a rough bed the measured gravity current's velocities were observed to be lower than those realized on a smooth bed. The observed general trend is that

an increase of bed's roughness causes a decrease of the front speed.

REFERENCES

Adduce, C., Sciortino, G., Proietti, S. 2009. Gravity currents produced by lock-exchange: experiments and simulations with a two layer shallow-water model with entrainment. Journal of Hydraulic Engineering (in revision).

Cenedese, C., Adduce C. 2008. Mixing in a density driven current flowing down a slope in a rotating fluid. J. Fluid Mech., 604, 369-388.

Huppert, H. E. 1982. The propagation of two-dimensional and axisymmetric viscous gravity currents over a rigid horizontal surface. J. Fluid Mech., 121, 43-58.

La Rocca, M., Adduce C.,Sciortino, G., Bateman Pinzon, A. 2008. Experimental and numerical simulation of three-dimensional gravity currents on smooth and rough bottom. Phys. Fluids, 20, 106603.

Marino, B. M., Thomas, L.P., Linden, P. F. 2005. The front condition of gravity currents. J. Fluid Mech., 536, 49-78.

Rottman, J. W., Simpson, J. E. 1983. Gravity currents produced by instantaneous releases of a heavy fluid in a rectangular channel. J. Fluid Mech., 135, 95-110.

Shin, J. O., Dalziel, S. B., Linden, P. F., 2004. Gravity currents produced by lock-exchange. J. Fluid mech., 521, 1-34.

Simpson, J. E. 1997. Gravity currents in the environment and laboratory. Cambridge University Press, Cambridge.